ARTICLE

Creating a Library of Complex Metallic Nanostructures *via* Harnessing Pattern Transformation of a Single PDMS Membrane

Ying Zhang,[†,§] Jason C Reed,[‡,§] and Shu Yang[†,*]

[†]Department of Materials Science and Engineering, University of Pennsylvania, Philadelphia, Pennsylvania 19104, and [‡]Department of Materials Science and Engineering, Cornell University, Ithaca, New York 14850. [§]These authors contributed equally to this work.

ABSTRACT By harnessing the elastic instability in a single PDMS membrane consisting of a square lattice array of circular pores, we fabricated a library of complex nanostructures in Au with variable feature size, connectivity, and geometry, including arrays of diamond-plate patterns (or elliptic herringbones), compound structures of circular dots and elliptical lines, heartbeat waves, aligned ovals, and a rhombus lattice of holes and lines. This was achieved first by swelling the PDMS membrane, followed by convective assembly of nanoparticles on the membrane. By taking advantage of the unique 3-D topography of the nanoparticle film and its photoresist replica, we could gradually etch the photoresist film to vary the feature size and connectivity of the underlying Au patterns. Further, through a combination of mechanical stretching (at different strain levels and stretching angles) and solvent swelling of the same PDMS membrane, we created a richer library of complex patterns in Au without application of new masters.

KEYWORDS: elastic instability · PDMS membranes · complex nanostructures in Au · swelling · pattern transfer · nanoparticle film · 3-D topography

The increasing interest in discovering and understanding new properties and phenomena of smaller and more sophisticated structures has stimulated extensive effort to develop new patterning techniques that will allow for fast and economical processes to create nanoscale structures without compromising high resolution features. Depending on the size, shape, and array geometry, nanostructured materials have the potential to impact a broad array of technological applications, including data storage, photonics, phononics, organic electronics, and sensing. For example, anisotropic unit cells are of interest for lasing with controlled polarization mode,[1] and photonic[2] and phononic[3,4] bandgap properties. Geometry-dependent, localized surface plasmon resonances (LSPR)[5] observed in metallic (*e.g.*, Au, Ag) nanostructures are of interest for light amplification, focusing, and coupling, as well as chemical and biological sensors.[6−12] Recently, a hybrid plasmonic nanoparticle, with a shape resembling a grain of rice, has been demonstrated to possess far more geometrically sensitive tunability than either a nanorod or a nanoshell while exhibiting significantly larger local field intensity enhancements.[13,14] These nanostructures are typically patterned *via* e-beam lithography or nonconventional lithography techniques, including microcontact printing (μCP),[15,16] nanoimprint lithography (NIL),[17] capillary force lithography (CFL),[18,19] and nanosphere lithography.[20] Recently, novel techniques, such as nanoskiving,[21,22] and nanotransfer edge printing,[23] have also been demonstrated to fabricate arrays of complex metallic nanostructures.

While considerable effort has been undertaken to develop advanced nanofabrication tools, a set of different masks or masters are often required in a production of nanostructures with different feature size and layout, which could contribute a significant portion of the time and total cost for the nanomanufacturing. It will be attractive to produce highly uniform nanostructures with tunable feature size and geometry using a single master/mold. It has been demonstrated in CFL that by controlling the capillary rise within the mold, a curved resist surface can be created, which serves as a tunable etch mask to transfer pattern metallic nanostructures with variable feature size and morphology.[18,19,24]

Recently, a few groups have explored the elastic deformation of poly(dimethylsiloxane) (PDMS) films to create new patterns that are different from the original master and with smaller feature sizes.[25−29] A patterned PDMS, replicated from a master that is fabricated by conventional photoli-

*Address correspondence to shuyang@seas.upenn.edu.

Received for review June 19, 2009 and accepted July 23, 2009.

Published online August 3, 2009.
10.1021/nn900650n CCC: $40.75

thography or e-beam lithography, has been widely used as a flexible stamp, mold, or mask to generate micro- and nanostructures in a wide range of materials on both flat and nonplanar substrates.[30,31] However, the elastic nature of soft PDMS (Young's modulus of 1−3 MPa) also makes the patterns prone to deformation under an external force or by exposure to an organic solvent.[32] By harnessing such instabilities, for example, roof collapse or "sagging" of PDMS molds when overpressure contact printing, researchers have successfully reduced the pattern size from ~10 μm to ~1 μm and form new patterns that differ from the original mold.[27,28] Through multiple compression, bending,or stretching of a PDMS mold, complex patterns have been created with feature size reduced from ~1.6 μm to ~200 nm.[25,26] By solvent swelling or uniaxial compression induced instabilities, we and others have triggered pattern transformation of porous PDMS membranes and elasto-plastic solids with periodic hole array to produce a wide range of orientationally modulated two-dimensional (2-D) complex patterns in nanoparticle films and polymers, respectively.[3,4,29,33−36] Specifically, by the combination of solvent swelling and convective assembly of nanoparticles, we demonstrate formation of complex patterns with sub-100 nm features with anisotropic unit cells over cm^2 regions in a single step.[29]

Interestingly, the nanoparticle films assembled from the swollen PDMS membranes are not flat but possess three-dimensional (3-D) surface topography: film thickness is the highest at the center of each elliptical unit, which gradually slopes down toward the center of the square lattice unit cell. By taking advantage of (1) the versatility and dramatic size reduction of the pattern transformation in PDMS membranes and (2) 3-D topography in the nanoparticle films, here, we demonstrate patterning of a library of complex nanostructures in Au with variable feature size, connectivity, and geometry, including arrays of diamond-plate patterns (continuous porous film and isolated ellipses), compound structures of circular dots and elliptical lines, heartbeat waves, aligned ovals, and a rhombus lattice of holes and lines, all from a *single* PDMS membrane consisting of a square lattice array of circular pores. This is achieved by replicating the 3-D topography from the nanoparticle film to an SU-8 photoresist film, which is then used as an etch mask to transfer patterns into a Au film through sequential resist etching and Au etching, followed by resist lift-off. Because the SU-8 film has an undulating thickness within each unit cell, the amount of resist remaining on the substrate will be a function of resist etching time, thus, allowing us to control the features size and connectivity of the produced Au patterns. We envision that the method presented here will offer a low-cost and efficient tool in manufacturing of functional nanostructures from a wide range of materials, including polymers, semiconductors, metals, and composites, which potentially will advance electronic, optical, microfluidic devices, sensors, and biochips.

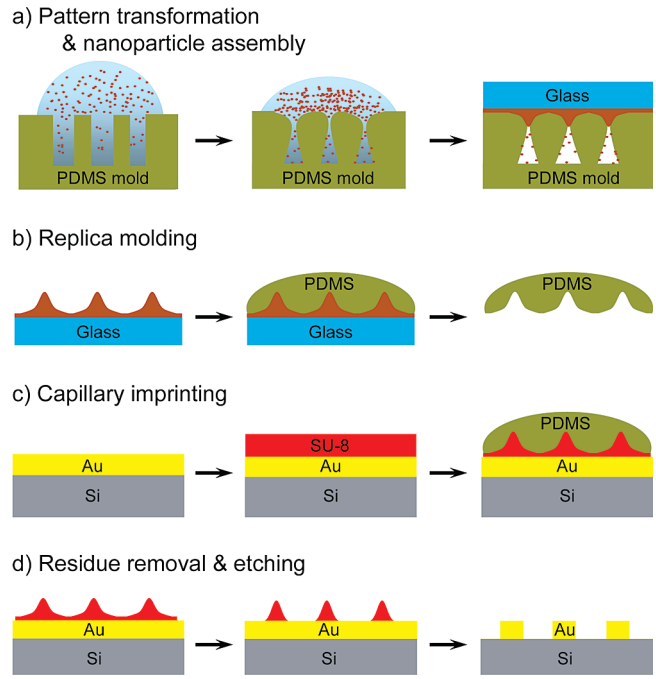

Figure 1. Schematic illustration of the fabrication process to produce Au nanostructures using SU-8 patterns as etch masks: (a) solvent swelling induced pattern transformation was captured by convective assembly of Fe_3O_4 nanoparticles; (b) patterned nanoparticle film was replicated into PDMS; (c) patterned SU-8 photoresist was imprinted from PDMS on a gold substrate; (d) SU-8 resist film was etched gradually by O_2 plasma to expose the underlying gold film, followed by gold etching and resist lift-off to obtain the patterned gold nanostructures.

RESULTS AND DISCUSSIONS

Figure 1 illustrates the fabrication procedure to create various patterned arrays of Au nanostructures from a *single* PDMS membrane. First, a nanoparticle film was convectively assembled on a solvent-deformed PDMS membrane. The nanoparticle film was then transferred to glass, which served as a master for pattern transfer of the 3-D topography into a SU-8 photoresist film through capillary imprinting *via* a PDMS mold. Last, the patterned SU-8 film was gradually etched, followed by Au etching and resist lift-off, resulting in Au nanostructures with different feature size and connectivity.

Previously, we have reported solvent swelling-induced pattern transformation in PDMS membrane with high aspect-ratio (AR = pore depth/diameter, 2−20), circular pores (pore diameter of 350 nm to 2 μm) in a square lattice array.[29] To capture the deformed pattern, we disperse Fe_3O_4 nanoparticles (~10 nm in diameter) in toluene and apply the solution to the surface of PDMS membrane. As the PDMS film swells, the square arrayed pores are elastically deformed to a diamond-plate pattern with elliptical lines orthogonal to each other (Figure 2a,b). The swelling causes a dramatic reduction of feature size, where the width of each elliptic nanoparticle deposit (78 nm) is smaller

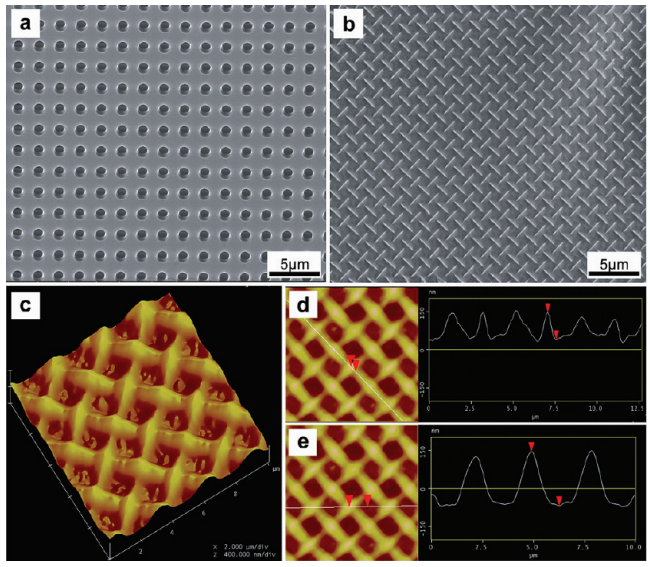

Figure 2. (a) SEM image of the original PDMS membrane with 1 μm pore size, 2 μm spacing and 9 μm depth; (b) SEM image of the diamond-plate nanoparticle film assembled from swollen PDMS membrane shown in panel a. (c−e) AFM images of the nanoparticle film shown in panel b: (c) 3-D view of surface topography; (d) AFM sectional height analysis along the minor axis of individual elliptical slit. The height from center to valley gradually decreased by ~104 nm; (e) AFM sectional height analysis cross the center of elliptical slit to the center of four neighboring units. The height decreased by ~213 nm. All AFM images are 10 × 10 μm².

than one-tenth the diameter of the initial pore (1 μm).[29] During the deformation, convective assembly of the nanoparticles follows and packs into the deformed pores, which faithfully prints the emergent patterns (Figure 1a). The pattern persists uniformly over a large area (up to a few cm², dependent on the size of the original master). Since the emergent pattern is the result of energy minimization of the neighboring pores

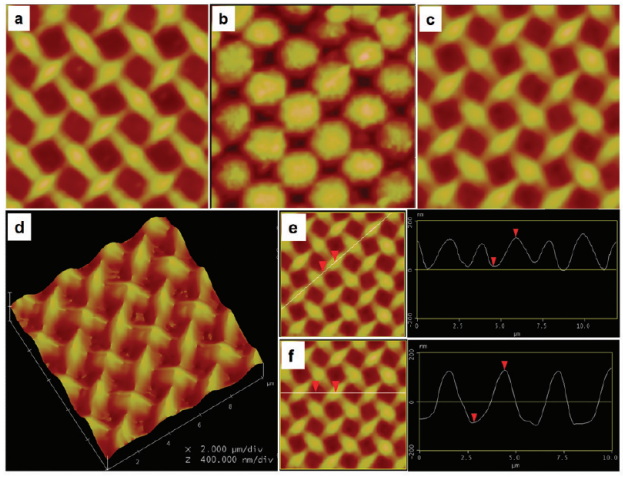

Figure 3. (a) AFM image of nanoparticle film; (b) AFM image of PDMS mold replicated from the nanoparticles film. (c−f) AFM images of SU-8 photoresist patterns imprinted from PDMS mold: (d) AFM 3-D view of surface topography of SU-8 photoresist pattern; (e) AFM sectional height analysis along the minor axis of individual elliptical slit. The height from center to valley gradually decreased by ~116 nm; (f) AFM sectional height analysis cross the center of elliptical slit to the center of four neighboring units. The height gradually decreased by ~216 nm. All AFM images are 10 × 10 μm².

upon deformation,[29,33,35] the pattern transformation should apply at all length scales. Indeed, the resulting diamond-plate has also been observed from square lattice arrays of millimeter size holes in elastomeric cellular solids,[33] and elastoplastic membrane with pore size of 190 nm[35] when they are subjected to compressive stress. Further, the degree of swelling of PDMS membranes can be controlled either by swelling time or by use of different organic solvents[37] and liquid monomers,[2] which in turn varies the osmotic pressure and compressive strain imposed to the PDMS membranes to alter the feature size of the resulting patterns. For example, we showed that fatter ellipses were obtained from poly(ethylene glycol dimethacrylate) (PEGDMA) films polymerized on the PDMS membrane than those from Fe_3O_4 nanoparticle assemblies because in the latter case toluene produced a much larger volume expansion ratio, (as much as 130%),[37] thereby deforming the pores more than the liquid monomers (*e.g.*, EGDMA).

As a proof-of-concept, here, we used a PDMS membrane consisting of square array of pores (pore diameter = 1 μm, pore depth = 9 μm, and lateral spacing = 2 μm) for pattern transformation and nanoparticle assembly (Figure 2). As seen from the 3-D view of atomic force microscopy (AFM) images, the nanoparticle film has a mountain-like morphology with continuous height variation that centered around the elliptical slits (Figure 2c−e). This is because the particle concentration should be the highest within the pores, whereas deposition of nanoparticles also occurred in the areas surrounding the pores during the convective assembly. According to the cross-section analysis, from the center (the highest region) to the edge of the minor axis of each individual elliptical unit, which is adjacent to the neighboring orthogonal ones, the height change is ~104 nm (Figure 2d), and the height change from the center of each elliptic unit to the center of four neighboring units (the lowest region) is ~213 nm (Figure 2e). Here, we exploited the application of the unique 3-D topography of the deformed patterns originated from a single PDMS membrane for fabrication of various complex patterns of metal nanostructures with variable size and connectivity.

Because the nanoparticles were assembled together through weak van der Waals forces, they tended to come off in the subsequent PDMS molding and peeling steps. To enhance the bonding between particles and the structure stability, we annealed the nanoparticle film at 200 °C for 10 min in air. The nanoparticle film was then replicated to a photoresist film by capillary imprinting *via* the PDMS mold at an elevated temperature (Figure 1b,c). Before this, a uniform Au film (30 nm thick) was thermally deposited on a clean silicon wafer, followed by spin coating of a thin film of SU-8 (225 nm thick) onto Au. Here, we cast SU-8 film with thickness matching the height of the nanoparticle film. Therefore, during the subsequent capillary imprinting,

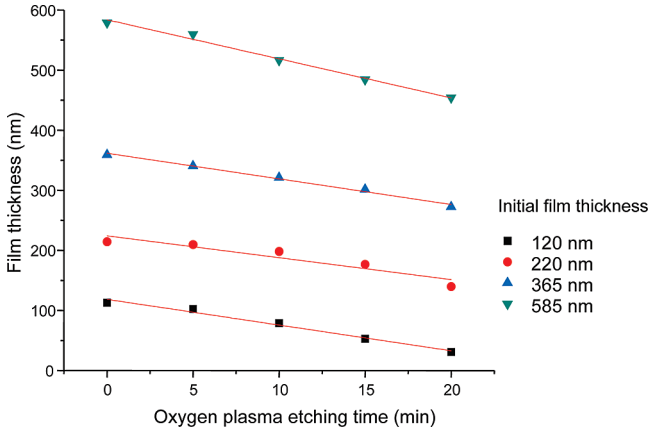

Figure 4. Oxygen plasma etching rate of SU-8 films with different initial thickness.

little residual film would remain on the substrate, which should be removed before pattern transfer. SU-8, a commercially available negative-tone photoresist, was chosen for pattern transfer because it is both thermoplastic (T_g, 50 °C and T_m, 82 °C, un-cross-linked) and etchable by O_2 plasma in a linear fashion. At 95 °C (above T_g), SU-8 has a low viscosity ($\eta \approx 5$ Pa · s). When the PDMS mold was slightly pressed against the SU-8 film, the viscous resist completely infiltrated the channels of the PDMS mold within seconds through capillary action.[38−40] After cooling to room temperature, the SU-8 film solidified and replicated the 3-D topography of nanoparticle film. Figure 3 shows AFM images at different stages of pattern transfer. By comparing the topography of SU-8 film with that of the initial nanoparticle film (Figure 2c−e), it is clear that the 3-D topography of the transformed pattern of the nanoparticle film faithfully replicated to SU-8.

We then used the imprinted SU-8 films as an etch mask to transfer patterns into Au films (Figure 1d). In the case of pattern transfer from a conventional resist pattern, which typically has a nearly vertical side-wall and uniform film thickness, the resulting pattern should have the same feature size and geometry as that of the original resist pattern. In our system, because the SU-8 film has an undulated film thickness from each elliptic unit center to the edge, we expect that the 3-D gradient topography will offer a new dimension for creating a range of metal patterns with variable feature size and morphology simply by changing the resist etching time, which gradually exposes the underlying Au film without using a series of sophisticated photomasks. Recently, several groups have employed such gradient etching effect in capillary force lithography as an elegant method to control the final pattern size and morphology, where the curved surface profile is generated due to capillary rise.[18,19,24]

During capillary imprinting, a thin residue layer (~100 nm) always occurred, which was first removed by O_2 plasma etching. To determine O_2 plasma etching rate, the SU-8 films prepared with different film thicknesses were subjected to etching at variable time. As seen in Figure 4, the SU-8 film was etched at a constant rate, ~ 5 nm/min. Therefore, we can control the thickness and morphology of the remaining resist, and in turn, the Au nanostructures. First, the thinnest region of resist film, that is, the center of the unit cell, was etched away. As plasma etching continued, more and more Au area was exposed. After each stage of resist etching, the exposed Au area was etched away by Au

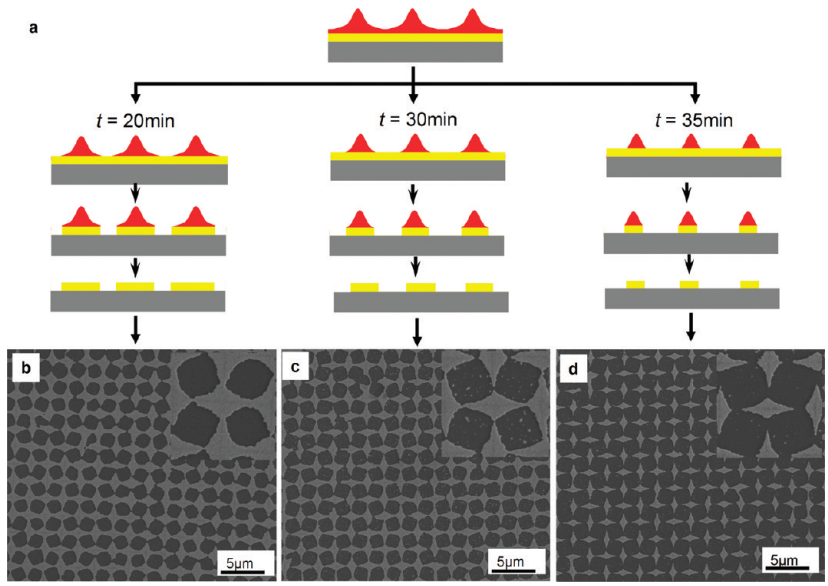

Figure 5. Various Au patterns obtained by etching the SU-8 films at different amount of time. (a) Schematic illustration of the fabrication process and effect of resist etching time to the resulting Au patterns. (b−d) SEM images of Au patterns obtained at different resist etching time: (b) 20, (c) 30, and (d) 35 min. The insets are enlarged view with area size 4 × 4 μm².

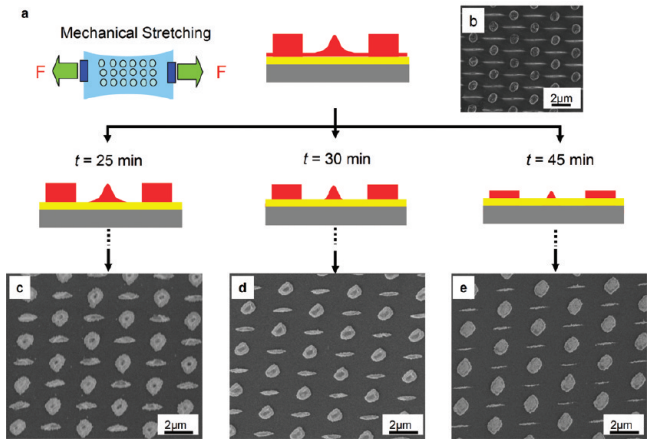

Figure 6. Various Au patterns obtained by etching SU-8 resist films consisting of a compound lattice of lines and circles at variable time. The SU-8 resist patterns were replicated from the nanoparticle films assembled on PDMS membranes when stretched along the lattice axis at $\varepsilon = 30-50\%$: (a) schematic illustration of the fabrication process and effect of resist etching time; (b) SEM image of the nanoparticle film. (c–e) SEM images of Au nanostructures obtained at different resist etching time: (c) 25, (d) 30, and (e) 45 min.

etchant, followed by resist lift-off to obtain the Au nanostructures (Figure 5a).

As seen in Figure 5b, after 20 min of resist etching, only the center region of four neighboring elliptic units were exposed, whereas most ridges remained connected to each other; therefore, a square-arrayed porous Au film was obtained. When the plasma etching time was increased to 30 min, the resist film was thinner and exposed more Au between the ellipses, yielding a just-connected Au film (Figure 5c). When the etching time was increased to 35 min, the connecting regions between neighboring ellipses were completely exposed, leaving a diamond-plate pattern with isolated nanospears resembling the original nanoparticle film (Figure 5d). Along with the pattern morphology change from a square-array porous membrane to a diamond-plate pattern in Au with increasing etching time, the pattern feature size also gradually decreased due to the reduced size of the etch mask. For example, each tip of each elliptic unit is very sharp, <50 nm wide, a feature size that is difficult to achieve by conventional photolithography. The continuing etching process is highly uniform over the whole sample area.

In addition to swelling-induce elastic deformation, we also combined swelling and mechanical stretching of the PDMS membrane along a lattice direction at different strain levels, therefore, exerting an external force favoring alignment along the strain direction to compete with the internal stresses caused by swelling.[29] By varying the strength of the external stress or the stretching angle with respect to the lattice axis, we created an even richer library of morphologies in nanoparticle films, including slightly distorted diamond-plate patterns, compound structures of circles and lines, a rectangular lattice of aligned ovals, and a rectangular line pattern (stretched 45° *vs* lattice axis). Accordingly, such patterns can be transferred to metallic films.

Figure 6 shows the Au pattern etched from the compound structure consisting of circles and lines at different etching time. The compound structures were created from PDMS membrane stretched at $\varepsilon = 30\%-50\%$ along the lattice axis (Figure 6b). It is interesting to note that as the oxygen plasma time was increased from 25 to 45 min, the circular dots did not show significant change in morphology and size, whereas the line pattern became narrower, whose width was decreased from 600 nm (Figure 6b) to 100 nm (Figure 6d). The difference in the etching behavior between circles and lines can be explained by the difference in the morphology of the nanoparticle film master: the nanoparticle (and resist) film at the circles was in the shape of cylindrical pillars with rather vertical sidewalls whereas at the line pattern region, a wedge-like sidewall was present. Thus, as the etching time increased, the height of the pillars decreased without changing the area of resist covering the Au. In contrast, near the line pattern region the height of nanoparticle assembly and resist film decreased continuously similar to that seen in Figures 2 and 3, therefore, both change of morphology and feature size of the resist and underlying Au pattern were observed.

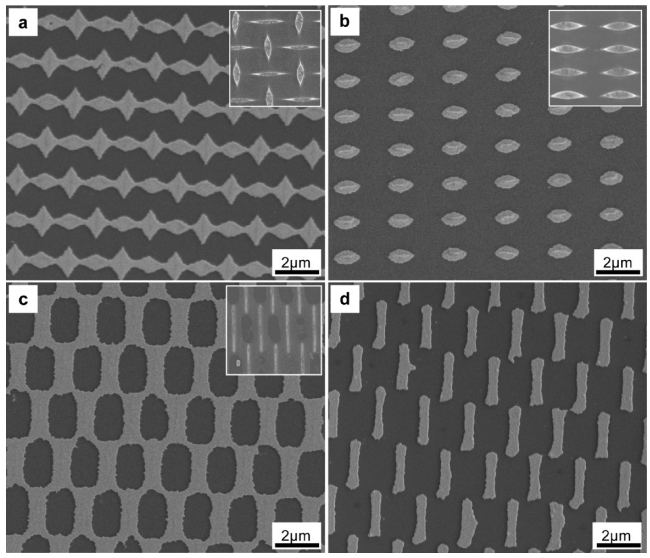

Figure 7. SEM images of different Au patterns obtained from nanoparticle films by swelling PDMS membranes stretched at various conditions: (a) stretching PDMS membrane along lattice axis with $\varepsilon = 10-30\%$ and the resist etching time is 35 min; (b) stretching PDMS membrane along lattice axis with $\varepsilon > 50\%$ with 35 min resist etching time. (c,d) Stretching PDMS membrane along 45° angle in respect to the lattice axis, and $\varepsilon = 64\%$ at different resist etching time: (c) 25 and (d) 45 min. The insets are corresponding nanoparticle films with area size 3 × 3 μm^2.

Further, by varying the stretching strain level and direction, we generated even more Au pattern morphologies in combination with resist etching time (Figure 7). For example, a highly undulated pattern with heartbeat waves were obtained from the slightly distorted diamond-plate master pattern ($\varepsilon \approx 10-30\%$ strain along the lattice axis) (Figure 7a). When ε was increased

to >50% along the lattice axis, a rectangular lattice of aligned ovals were obtained and transferred to the Au film (Figure 7b). When stretching the PDMS membrane with $\varepsilon = 64\%$ in the direction of 45° to the lattice axis, followed by solvent swelling, the lattice symmetry changed from square to rhombus (Figure 7c inset). Similar to the pattern transfer illustrated in diamond-plate patterns, a porous Au film was obtained when the oxygen plasma etching time was 25 min (Figure 7c). When the etching time was increased to 45 min, a rhombus lattice of isolated rectangular Au rods was obtained, where the long axis of rods were aligned in the stretching direction (Figure 7d). It is worth noting that all of the above shown Au nanostructures were created from deformation of a single PDMS membrane.

CONCLUSION

By harnessing the elastic instability in a PDMS membrane with periodic microscale pores, we created a series of nanoparticle films with complex patterns. These nanoparticle films then served as masters and the patterns of which were faithfully imprinted to a photoresist film, SU-8. These photoresist patterns were used as etch masks for pattern transfer to the underlying Au films to create a library of Au nanostructures. Because of the unique 3-D topography of the nanoparticle film and its photoresist replica, we could gradually etch the photoresist to control etch mask shape, connectivity, and feature size, thus varying the size and connectivity/morphology of the final Au nanopatterns. Further, through a combination of mechanical stretching (at different strain levels and stretching angles) and solvent swelling of the same PDMS membrane, we created a richer library of complex patterns in Au without application of sophisticated photopatterning tools or new masters. We believe the method described here potentially will offer an inexpensive, versatile, patterning technique for nanomanufacturing of various nanostructures in metals, semiconductors, and polymers/hybrids.

METHODS

Details of PDMS mold fabrication, and convective assembly of Fe_3O_4 nanoparticles on both nonstretched and mechanically stretched PDMS membranes have been reported previously.[29]

PDMS Replication of the Nanoparticle Films. The nanoparticle film was first transfer-printed onto a glass slide and lifted off from the PDMS membrane, followed by annealing at 200 °C for 10 min in air to promote bonding between nanoparticles and the glass. PDMS prepolymer was then poured over the nanoparticle film, cured at 65 °C for 4 h to replicate the nanoparticle film structure. The PDMS mold was carefully peeled off from the nanoparticle film and used in the following experiments without any further treatment.

Imprinting of the Deformed Patterns into SU-8 Photoresists. A silicon wafer was first cleaned with acetone and isopropanol, followed by oxygen plasma to remove any organic deposits. A thin layer of 30 nm Au (99.999%, 1−6 mm bead, Sigma Aldrich) and 3 nm Cr (99.995%, ~1 mm thick chip, Sigma Aldrich) adhesion layer was thermally evaporated at a rate of 1 Å/s at 5×10^{-7} torr onto the silicon wafer in a Thermionics VE-90 Thermal Evaporator. Negative photoresist SU-8 (40 wt % in γ-butyrolactone, Micro-Chem) was diluted to 6.8 wt % in cyclopentanone (99+%, Acros Organics) and spun onto the gold surface at 3000 rpm for 30 s, followed by soft baking at 65 °C for 2 min and 95 °C for 5 min, respectively. At 95 °C (above the T_g of SU-8), the PDMS mold was pressed into the viscous polymer film under a small pressure of 100 g/cm^2. After 5 min the sample was cooled down to room temperature, and PDMS mold was peeled off.

Pattern Transfer from SU-8 Films to Au Films. The patterned SU-8 polymer film was etched by oxygen plasma cleaner (PDC-001, Harrick Scientific Products, Inc.) at 29.6 W and 800 mtorr for a variable amount of time. The etching rate is estimated as 5 nm/min. After plasma etching, the exposed gold was removed by a gold etchant (Transene, Gold Etch - type TFA), which was diluted with DI water (1 mL etchant: 2 mL water) for 20 s, followed by rinsing with copious amounts of DI water. Afterward, the remaining SU-8 film was stripped by oxygen plasma to reveal the Au nanostructures.

Characterization. Scanning electron microscopy (SEM) images were obtained on FEI Strata DB235 with an acceleration voltage of 5 kV and spot size of 3. Atomic force microscopy (AFM) images were obtained on a Nanscope III AFM (Digital Instruments). The thickness of spin-coated SU-8 films was measured by Rudolph Auto El IV ellipsometer.

Acknowledgment. This work is supported in part by National Science Foundation (NSF) CAREER and CAREER/REU (JR) # DMR-0548070, and NSF/MRSEC # DMR-0520020. J.R. would also like to thank Dr. A. McGhie for overseeing the University of Pennsylvania LRSM-REU program. We are grateful to Prof. J. Kikkawa (Physics, Penn) for insightful discussion, which motivated this research.

REFERENCES AND NOTES

1. Noda, S.; Yokoyama, M.; Imada, M.; Chutinan, A.; Mochizuki, M. Polarization Mode Control of Two-Dimensional Photonic Crystal Laser by Unit Cell Structure Design. *Science* **2001**, *293*, 1123–1125.
2. Zhu, X.; Zhang, Y.; Chandra, D.; Cheng, S.-C.; Kikkawa, J. M.; Yang, S. Two-Dimensional Photonic Crystals with Anisotropic Unit Cells Imprinted from Poly(dimethylsiloxane) Membranes Under Elastic Deformation. *Appl. Phys. Lett.* **2008**, *93*, 161911–3.
3. Bertoldi, K.; Boyce, M. C. Mechanically Triggered Transformations of Phononic Band Gaps in Periodic Elastomeric Structures. *Phys. Rev. B* **2008**, *77*, 052105.
4. Jang, J.-H.; Koh, C. Y.; Bertoldi, K.; Boyce, M. C.; Thomas, E. L. Combining Pattern Instability and Shape-Memory Hysteresis for Phononic Switching. *Nano Lett.* **2009**, *9*, 2113–2119.
5. Willets, K. A.; Van Duyne, R. P. Localized Surface Plasmon Resonance Spectroscopy and Sensing. *Annu. Rev. Phys. Chem.* **2007**, *58*, 267–297.
6. Jung, L. S.; Campbell, C. T.; Chinowsky, T. M.; Mar, M. N.; Yee, S. S. Quantitative Interpretation of the Response of Surface Plasmon Resonance Sensors to Adsorbed Films. *Langmuir* **1998**, *14*, 5636–5648.
7. Haes, A. J.; Zou, S. L.; Schatz, G. C.; Van Duyne, R. P. A Nanoscale Optical Biosensor: The Long Range Distance Dependence of the Localized Surface Plasmon Resonance of Noble Metal Nanoparticles. *J. Phys. Chem. B* **2004**, *108*, 109–116.
8. Endo, T.; Kerman, K.; Nagatani, N.; Takamura, Y.; Tamiya, E. Label-Free Detection of Peptide Nucleic Acid-DNA Hybridization Using Localized Surface Plasmon Resonance Based Optical Biosensor. *Anal. Chem.* **2005**, *77*, 6976–6984.
9. Henzie, J.; Barton, J. E.; Stender, C. L.; Odom, T. W. Large-Area Nanoscale Patterning: Chemistry Meets Fabrication. *Acc. Chem. Res.* **2006**, *39*, 249–257.

10. Engheta, N. Circuits with Light at Nanoscales: Optical Nanocircuits Inspired by Metamaterials. *Science* **2007**, *317*, 1698–1702.
11. Lei, Y.; Cai, W. P.; Wilde, G. Highly Ordered Nanostructures with Tunable Size, Shape, and Properties: A New Way to Surface Nano-Patterning Using Ultra-thin Alumina Masks. *Prog. Mater. Sci.* **2007**, *52*, 465–539.
12. Anker, J. N.; Hall, W. P.; Lyandres, O.; Shah, N. C.; Zhao, J.; Van Duyne, R. P. Biosensing with Plasmonic Nanosensors. *Nat. Mater.* **2008**, *7*, 442–453.
13. Wang, H.; Brandl, D. W.; Le, F.; Nordlander, P.; Halas, N. J. Nanorice: A Hybrid Plasmonic Nanostructure. *Nano Lett.* **2006**, *6*, 827–832.
14. Wang, H.; Brandl, D. W.; Nordlander, P.; Halas, N. J. Plasmonic Nanostructures: Artificial Molecules. *Acc. Chem. Res.* **2007**, *40*, 53–62.
15. Xia, Y. N.; Whitesides, G. M. Use of Controlled Reactive Spreading of Liquid Alkanethiol on the Surface of Gold to Modify the Size of Features Produced by Microcontact Printing. *J. Am. Chem. Soc.* **1995**, *117*, 3274–3275.
16. Xia, Y. N.; Whitesides, G. M. Soft Lithography. *Annu. Rev. Mater. Sci.* **1998**, *28*, 153–184.
17. Lucas, B. D.; Kim, J. S.; Chin, C.; Guo, L. J. Nanoimprint Lithography Based Approach for the Fabrication of Large-Area, Uniformly Oriented Plasmonic Arrays. *Adv. Mater.* **2008**, *20*, 1129.
18. Suh, K. Y.; Kim, Y. S.; Lee, H. H. Capillary Force Lithography. *Adv. Mater.* **2001**, *13*, 1386–1389.
19. Bruinink, C. M.; Peter, M.; Maury, P. A.; De Boer, M.; Kuipers, L.; Huskens, J.; Reinhoudt, D. N. Capillary Force Lithography: Fabrication of Functional Polymer Templates as Versatile Tools for Nanolithography. *Adv. Funct. Mater.* **2006**, *16*, 1555–1565.
20. Chan, G. H.; Zhao, J.; Hicks, E. M.; Schatz, G. C.; Van Duyne, R. P. Plasmonic Properties of Copper Nanoparticles Fabricated by Nanosphere Lithography. *Nano Lett.* **2007**, *7*, 1947–1952.
21. Xu, Q.; Gates, B. D.; Whitesides, G. M. Fabrication of Metal Structures with Nanometer-Scale Lateral Dimensions by Sectioning Using a Microtome. *J. Am. Chem. Soc.* **2004**, *126*, 1332–1333.
22. Xu, Q.; Rioux, R. M.; Dickey, M. D.; Whitesides, G. M. Nanoskiving: A New Method to Produce Arrays of Nanostructures. *Acc. Chem. Res.* **2008**, *41*, 1566–1577.
23. Xue, M. Q.; Yang, Y. L.; Cao, T. B. Well-Positioned Metallic Nanostructures Fabricated by Nanotransfer Edge Printing. *Adv. Mater.* **2008**, *20*, 596–600.
24. Jung, J. M.; Stellacci, F.; Jung, H. T. Generation of Various Complex Patterned Structures from a Single Ellipsoidal Dot Prepattern by Capillary Force Lithography. *Adv. Mater.* **2007**, *19*, 4392–4398.
25. Xia, Y. N.; Kim, E.; Zhao, X. M.; Rogers, J. A.; Prentiss, M.; Whitesides, G. M. Complex Optical Surfaces Formed by Replica Molding Against Elastomeric Masters. *Science* **1996**, *273*, 347–349.
26. Xia, Y. N.; Whitesides, G. M. Extending Microcontact Printing as a Microlithographic Technique. *Langmuir* **1997**, *13*, 2059–2067.
27. Guo, Q. J.; Teng, X. W.; Yang, H. Overpressure Contact Printing. *Nano Lett.* **2004**, *4*, 1657–1662.
28. Fan, X.; Tran, D. T.; Brennan, D. P.; Oliver, S. R. J. Microfabrication Using Elastomeric Stamp Deformation. *J. Phys. Chem. B* **2006**, *110*, 11986–11990.
29. Zhang, Y.; Matsumoto, E. A.; Peter, A.; Lin, P. C.; Kamien, R. D.; Yang, S. One-Step Nanoscale Assembly of Complex Structures *via* Harnessing of Elastic Instability. *Nano Lett.* **2008**, *8*, 1192–1196.
30. Gates, B. D.; Xu, Q. B.; Love, J. C.; Wolfe, D. B.; Whitesides, G. M. Unconventional Nanofabrication. *Annu. Rev. Mater. Res.* **2004**, *34*, 339–372.
31. Geissler, M.; Xia, Y. N. Patterning: Principles and Some New Developments. *Adv. Mater.* **2004**, *16*, 1249–1269.
32. Hui, C. Y.; Jagota, A.; Lin, Y. Y.; Kramer, E. J. Constraints on Microcontact Printing Imposed by Stamp Deformation. *Langmuir* **2002**, *18*, 1394–1407.
33. Mullin, T.; Deschanel, S.; Bertoldi, K.; Boyce, M. C. Pattern Transformation Triggered by Deformation. *Phys. Rev. Lett.* **2007**, *99*, 084301.
34. Bertoldi, K.; Boyce, M. C.; Deschanel, S.; Prange, S. M.; Mullin, T. Mechanics of Deformation-Triggered Pattern Transformations and Superelastic Behavior in Periodic Elastomeric Structures. *J. Mech. Phys. Solids* **2008**, *56*, 2642–2668.
35. Singamaneni, S.; Bertoldi, K.; Chang, S.; Jang, J.-H.; Thomas, E. L.; Boyce, M. C.; Tsukruk, V. V. Instabilities and Pattern Transformation in Periodic, Porous Elastoplastic Solid Coatings. *ACS Appl. Mater. Interfaces* **2009**, *1*, 42–47.
36. Singamaneni, S.; Bertoldi, K.; Chang, S.; Jang, J. H.; Young, S. L.; Thomas, E. L.; Boyce, M. C.; Tsukruk, V. V. Bifurcated Mechanical Behavior of Deformed Periodic Porous Solids. *Adv. Funct. Mater.* **2009**, *19*, 1426–1436.
37. Lee, J. N.; Park, C.; Whitesides, G. M. Solvent Compatibility of Poly(dimethylsiloxane)-Based Microfluidic Devices. *Anal. Chem.* **2003**, *75*, 6544–6554.
38. Zhang, Y.; Lo, C. W.; Taylor, J. A.; Yang, S. Replica Molding of High-Aspect-Ratio Polymeric Nanopillar Arrays with High Fidelity. *Langmuir* **2006**, *22*, 8595–8601.
39. Pfeiffer, K.; Fink, A.; Gruetzner, G.; Bleidiessel, G.; Schulz, H.; Scheer, H. Multistep Profiles by Mix and Match of Nanoimprint and UV Lithography. *Microelecton. Eng.* **2001**, *57−8*, 381–387.
40. Cheng, X.; Guo, L. J. One-Step Lithography for Various Size Patterns with a Hybrid Mask-Mold. *Microelectron. Eng.* **2004**, *71*, 288–293.